Small-Scale Structure in the Stormtime Ring Current

Michael W. Liemohn

Atmospheric, Oceanic, and Space Sciences Department, University of Michigan, Ann Arbor

Pontus C. Brandt

Johns Hopkins University Applied Physics Laboratory, Laurel, Maryland

The partial ring current tries to limit itself through the electric field associated with the ionospheric closure currents. The relationship between the hot ion pressure peak and the electric potential structure is examined, and the negative feedback of the stormtime ring current on itself is discussed. To investigate this issue, simulation results for the magnetic storm of April 17, 2002 were analyzed. It was found that the small-scale well-and-peak potential pairs, formed when magnetotail plasma is injected or convected in to the inner magnetosphere, significantly change the near-Earth plasma distribution. Though the potential structures are not always visible in the potential distribution plots or energetic neutral atom images, their effect is noticeable because the main pressure peak is broken into many smaller peaks and the flow pattern of the hot ions is altered. The consequences of these partial ring current-induced potential structures were also discussed. In particular, subauroral polarization streams and injection flow channels were seen in the potential distributions at various times during the storm, formed when the small-scale electric field is aligned with the large-scale electric field in some local region.

1. INTRODUCTION

When hot plasma moves from the magnetotail into the inner magnetosphere, it adiabatically accelerates and thus undergoes additional gradient-curvature drift [*Alfvén and Fälthammar*, 1963]. During times of strong convection, this "partial ring current" easily dominates the plasma pressure in near-Earth space [e.g., *Akasofu and Chapman*, 1964; *Frank et al*., 1970]. It is a partial ring because the current does not go all the way around the Earth. Instead, the plasma is convected away from Earth on the dayside, is adiabatically de-energized, and then flows to the dayside magnetopause [*Takahashi et al*., 1990]. The resulting plasma morphology is a pressure crescent that extends across the nightside/dusk-side of the Earth [e.g., *Ejiri*, 1978; *Liemohn et al*., 2001a].

The perpendicular current flows along the pressure isobars, but it is inversely proportional to the local magnetic field strength [*Parker*, 1957, 2000]. When the current flow (that is, a pressure isobar) is not parallel to the magnetic field isocontours, currents must flow along the magnetic field to balance this inequality [*Vasyliunas*, 1970]. These field-aligned currents (FACs) flow in to and out of the ionosphere. There, the electric conductivity is high enough that the current can cross the field lines and close the circuit loop [e.g., *Farley*, 1959; *Banks and Kokarts*, 1973]. The latitude and longitude distribution of the conductivity, as well as the distribution of the sources and sinks (the FACs), determine the ionospheric current circulation [e.g., *Heppner*, 1972].

Title
Book Series
Copyright 200# XXXXXXXXXXX.
##.####/###GM##

These currents are directly related to the ionospheric electric fields through Ohm's law. Because the inner magnetospheric field lines can be treated as perfect conductors (no electric potential drop along them), the ionospheric electric fields map out to the inner magnetosphere and exert a force on the charged particles there. So, moving hot plasma into the inner magnetosphere by some electric field changes the electric field.

Several studies have examined the self-consistent feedback loop between the subauroral ionosphere and the inner magnetosphere. *Jaggi and Wolf* [1973] predicted severe distortions of the potential pattern near the Earth around local midnight. *Southwood and Wolf* [1978] showed that this feedback takes a few hours to readjust the plasma and the electric field into a stable balance. This final, quasi-equilibrium state is known as the shielding effect [*Spiro and Wolf*, 1984]. During this adjustment interval, under-shielding occurs where the high-latitude potential pattern penetrates to low latitudes [e.g., *Spiro et al*., 1988; *Fejer et al*., 1990]. Not only does the high-latitude pattern shift to lower latitudes, the subauroral potential pattern is distorted and often amplified, resulting in a different form of penetration electric field [e.g., *Ridley and Liemohn*, 2002]. The main feature of second kind of penetration field is a potential well near midnight. This potential well can be large and causes a severe alteration in the plasma drifts in this region [*Fok et al*., 2001, 2003; *Khazanov et al*., 2003; *Jordanova et al*., 2003; *Garner et al*., 2004; *Liemohn et al*., 2004].

Indeed, with every injection of a blob of plasma into the inner magnetosphere, a potential well develops at the eastern end of the pressure crescent and a potential peak develops at the western end (according to the physical process described above). Figure 1 shows a schematic illustration of this phenomenon. The electric fields point in toward the well and out away from the peak. Because the magnetic field in the magnetospheric equatorial plane points northward, the resulting plasma drifts are counter-clockwise around the well and clockwise around the peak. So, with every injection, a vortex pair is formed that alters the local flow of plasma. *Sazykin et al*. [2002] investigated similar vortices as a cause of structure in the hot plasma morphology. In that case, however, the vortices were from the interchange instability. The flow around the western end of the plasma pressure peak is said to be the cause of the skewed ion distributions (shifting the peak to the post-midnight sector) seen in the energetic neutral atom images [*Brandt et al*., 2002].

As seen in Figure 1, the flows from the twin vortices merge in the middle, creating an outward flow co-located with the peak of the pressure crescent. Therefore, the mere existence of the pressure peak creates a flow pattern

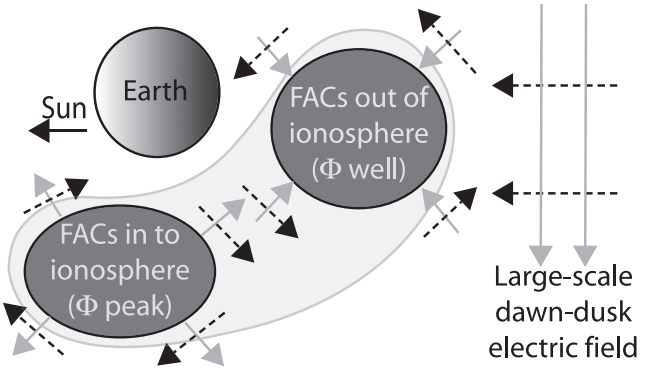

Figure 1. Schematic of the relationship between the partial ring current, the field-aligned closure currents, and the strong electric fields in the inner magnetosphere. The large, lightly-shaded region is an example partial ring current (out to some arbitrary isobar). The two darker shaded regions are the regions of strong field-aligned current (again, drawn out to some arbitrary FAC level). The lightly-shaded arrows show the electric fields associated with the large-scale potential difference (big arrows on the right), and the potential peak and well associated with the FAC regions. The dark, dashed arrows show the ExB drift direction for each electric field arrow.

that acts to expel the peak from the inner magnetosphere. However, only in the middle of the pressure crescent, where the two vortices meet, do strong outward flows exist. The rest of the pressure crescent does not experience expelling forces, and the ends of the crescent actually are pushes in towards the Earth.

The story above describes the basic scenario of what happens when hot plasma is moved into the inner magnetosphere. The details of this process, however, are not well understood. For instance, are any of these electric fields significant relative to the large-scale dawn-dusk convection electric field? Remember that at this time, shielding is broken down and the large-scale field can penetrate deep into the inner magnetosphere (that is, to low latitudes). If so, when are the vortex electric fields significant and how big are they?

The study presented here addresses these questions with the use of a kinetic transport model. A particular case study, the April 17, 2002 magnetic storm, will be examined in detail in the next section. The following section gives a general discussion of these results, and relates it to previous work on the inner magnetospheric electric field structure. It is found that the ring current is self-limiting; the fields are locally quite strong and the net result of the negative feedback loop is that the initially-large pressure peaks are broken up into small-scale peaks and valleys, eventually forming a rough but symmetric ring current in the late recovery phase of the storm.

2. EXAMPLE CASE STUDY: THE APRIL 17, 2002 STORM

The April 17, 2002 magnetic storm was caused by the initial interplanetary shock and sheath passage of the multi-storm sequence that month. At least 4 interplanetary coronal mass ejections (ICMEs) struck the magnetosphere from the 17th to the 24th, with varying degrees of geomagnetic activity associated with each hit. The first shock arrived at ~11:55 UT on April 17, and the subsequent sheath passage lasted over 12 hours (followed by a magnetic cloud, which caused the second storm in the sequence). The solar wind velocity jumped from ~350 km/s to ~500 km/s, and the solar wind density exceeded 20 cm^{-3} for over 6 hours, with spikes up to 60 cm^{-3}. The interplanetary magnetic field (IMF) oscillated wildly during the sheath, especially during the first 8 hours, with southward excursions of up to −25 nT. This solar wind disturbance caused a magnetic storm with a Dst minimum value of −105 nT (at 17:00 UT), recovering to roughly -50 nT early on April 18 (when the cloud arrived and the second storm began). *Liemohn et al*. [2004] provides more details of the solar wind and geophysical conditions during this event.

This storm was modeled with the version of the ring current-atmosphere interaction model (RAM) described by *Liemohn et al*. [2004]. This version of RAM, based on earlier versions by *Fok et al*. [1993], *Jordanova et al*. [1996], and *Liemohn et al*. [1999], solves the time-dependent, gyration- and bounce-averaged kinetic equation for the phase-space density $f(t, R, \varphi, E, \mu_0)$ of one or more ring current species. The five independent variables are time, geocentric radial distance in the equatorial plane, magnetic local time, kinetic energy, and cosine of the equatorial pitch angle. The code includes collisionless drifts, energy loss and pitch angle scattering due to Coulomb collisions with the thermal plasma (densities from the *Ober et al*. [1997] model), charge exchange loss with the hydrogen geocorona (densities from the *Rairden et al*. [1986] model), and precipitative loss to the upper atmosphere. Solution of the kinetic equation is accomplished by replacing the derivatives with second-order accurate, finite volume, numerical operators. Note that this is not a particle-tracking code but actually a "fluid" calculation, with the "fluids" being the several million grid cells in phase space for each plasma species.

The source term for the phase space density calculated by RAM is the outer simulation boundary, where observed particle fluxes from the magnetospheric plasma analyzer (MPA) [*McComas et al*., 1993] and synchronously orbiting plasma analyzer (SOPA) [*Belian et al*., 1992] instruments on the LANL geosynchronous-orbit satellites are applied as input functions. Variations in the observed plasma sheet density at a single satellite are assumed to represent temporal variations of a spatially uniform nightside plasma sheet. Data gaps are filled in using data from earlier and later local times if the ion data is not significantly degraded by losses. The composition of the inner plasma sheet is assumed to vary with solar and magnetic activity according to the statistical relationship derived by *Young et al*. [1982]. Additional details of the present state of RAM are presented by *Liemohn et al*. [1999, 2001a, b, 2004].

The electric field description is an important component of RAM. Simulations with two different field descriptions are discussed in this study. The first is a self-consistent electric field inside the simulation domain. That is, field-aligned currents calculated from the hot ion results are used as a source term in a Poisson equation solution for the ionospheric potential. A high-latitude boundary condition from the Weimer potential model [*Weimer*, 1996] is used at ~72°. A time-varying conductance pattern is also prescribed. Specifically, a static but spatially nonuniform dayside and nightside conductance pattern is defined, and then a dynamic "smooth auroral oval" ring of conductance is also applied. These rings (north and south hemispheres) vary with the location and strength of the field-aligned currents calculated from RAM. Please see *Ridley et al*. [2004] and *Liemohn et al*. [2004] for additional details of the conductance pattern. The second electric field description used in this study is the *Weimer* [1996] pattern, applied everywhere instead of just at the high-latitude boundary. Therefore, the two potential descriptions have the same large-scale, dawn-dusk electric field, but different inner magnetospheric patterns.

2.1. Hot Ion Pressures

Plates 1 and 2 show the calculated hot ion (H^+ plus O^+) pressure distributions at 12 times throughout the April 17 magnetic storm. The maximum total energy content (that is, the integral of this pressure over the simulation domain) occurs at 17:00 UT for the self-consistent electric field run (Plate 1) and at 17:30 UT for the Weimer-96 run (Plate 2). The main similarity between Plates 1 and 2 is that the pressure peaks in the evening sector throughout the main phase and first few hours of the recovery phase, but then this peak weakens and moves around the Earth during the late recovery phase. A primary difference between these simulation results is that Plate 1 shows far more small-scale structure than seen in Plate 2. The pressure peak in Plate 2 is always a well-defined, very smooth crescent. It is highly asymmetric during the main phase of the storm (before the peak), and relaxes to a nearly symmetric local time pressure distribution by 21:00 UT.

In contrast, Plate 1 reveals a somewhat larger symmetric ring current component during the main phase but a stronger

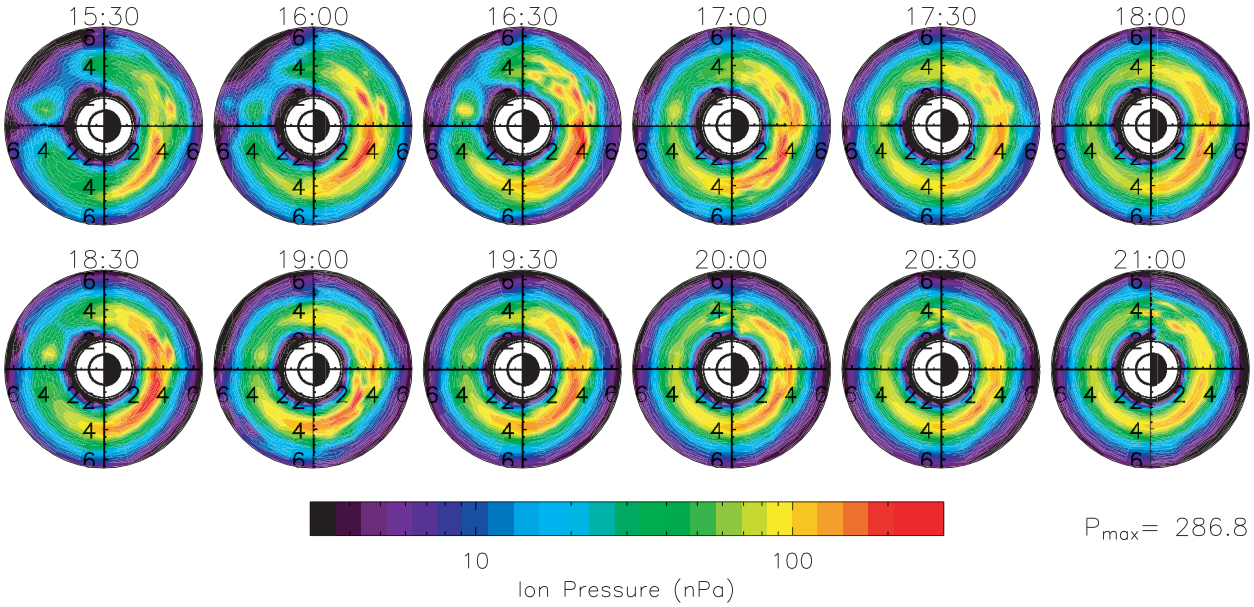

Plate 1. Equatorial plane plasma pressures in the inner magnetosphere for the simulation with the self-consistent electric field description throughout the simulation domain. The view in each subplot is over the north pole, with the sun to the left and dusk down, with distances in Earth radii. The maximum hot ion pressure in these 12 dial plots is listed in the lower right.

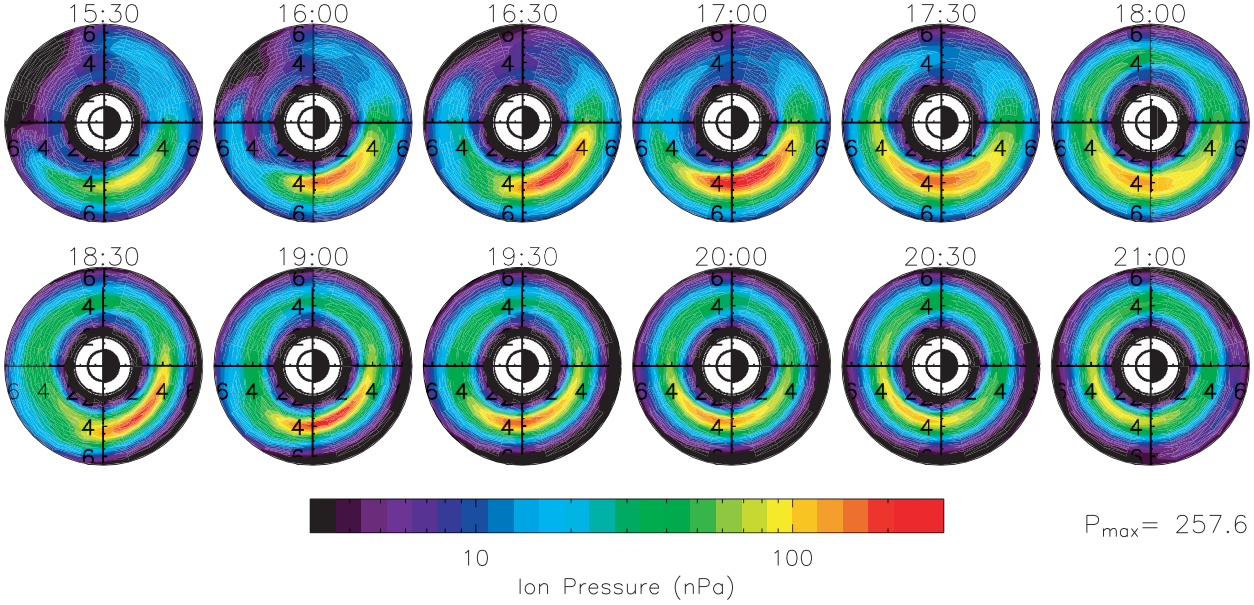

Plate 2. Like Plate 1, plasma pressures in the inner magnetosphere for the simulation with the Weimer-96 electric field description throughout the simulation domain.

partial ring current component in the recovery phase (relative to that in Plate 2). There are many localized peaks within the main pressure peak. In particular, it appears that the pressure peaks are azimuthally long and radially narrow on the duskside inner magnetosphere but more spot-like in structure on the dawnside. Another primary difference between Plates 1 and 2 is that the pressure peak in the self-consistent run (Plate 1) extends much farther eastward (toward dawn) than that created by the Weimer-96 electric fields.

In general, the hot ion pressure values from the two results are quite similar in magnitude. The peak value for all 12 times shown (listed in the lower right corner of each plate) is ~10% bigger for the self-consistent electric field result than for the Weimer-96 electric field result. The reason for this is that the vortices trap some of the plasma on the nightside and don't let it convect as easily through the inner magnetosphere. There is less convective trapping with the Weimer E-field. The rotational flow of the vortices also means that particles are injected more deeply in localized regions of the nightside, which leads to extra adiabatic acceleration and a (slightly) higher peak pressure value.

2.2. Electric Potentials

Figures 2 and 3 show the electric potential distribution in the simulation domain for the self-consistent and Weimer-96 simulations, respectively. Figure 2 contains far more small-scale potential structure than does Figure 3. The main feature in the plots of Figure 3 that resembles the potential well-and-peak pairs from plasma injection is the extension of the duskside potential well over to the midnight meridian near 4 R_E. Otherwise, Figure 3 shows the standard two-cell convection pattern (a dawn-to-dusk electric field) that is very strong in the main phase of the storm and tapers off to much lower values in the recovery phase.

Figure 2 also has this basic pattern, with a strong large-scale convection field in the main phase that weakens in the recovery phase. However, it also contains several (sometimes many) local maxima and minima. At 17:00 UT, the brief interval of weakened large-scale convection reveals a rather strong overshielding potential pattern throughout the inner magnetosphere (causing reverse convection) and significant small-scale potential structure near dusk. When the large-scale convection field is strong, however, the only consistent feature is that seen in the Weimer-96 potential patterns: the extension of the duskside potential well towards (or past) midnight near the Earth. A substantial difference between Figure 2 and 3 is that the complexity of the self-consistent potential distribution persists throughout the recovery phase of the storm. In fact, because of the weakening large-scale convection field, the potential wells and peaks from the localized pressure peaks are much more noticeable in the lower row of plots in Plate 4 than in the upper row.

2.3. Observational Perspective

It is useful to consider what data might be able to tell us about the existence of these small-scale features in the hot ion

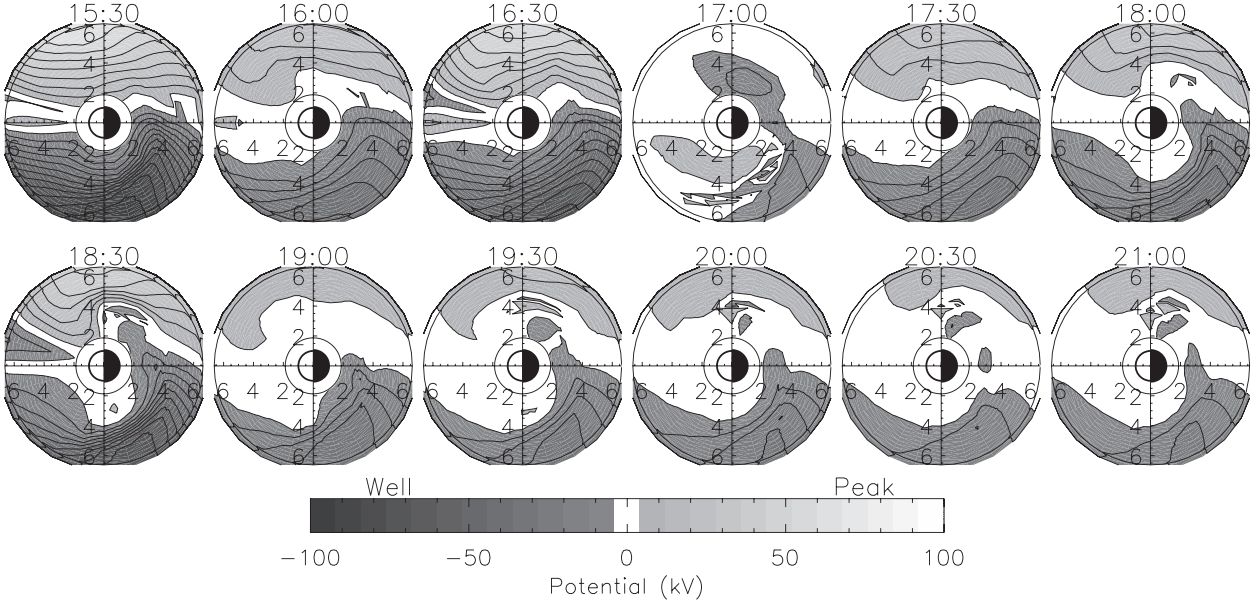

Figure 2. Electric potentials in the inner magnetosphere for the simulation with the self-consistent electric fields. The format is like Plate 1. Contours are drawn every 8 kV.

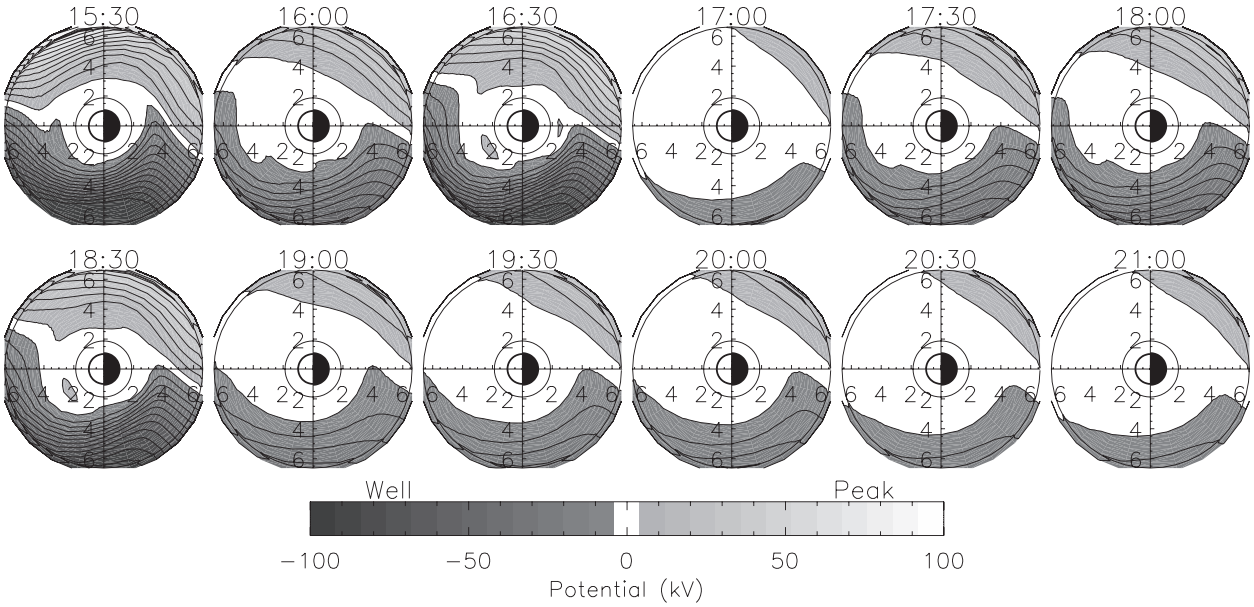

Figure 3. Like Figure 2, electric potentials in the inner magnetosphere for the simulation with the Weimer-96 electric fields.

pressure distribution of the stormtime ring current. A convenient data set is that from the HENA instrument [*Mitchell et al*., 2000] onboard the IMAGE spacecraft [*Burch*, 2000]. This instrument records energetic neutral atoms, a bi-product of the charge exchange decay mechanism of the ring current, and is able to view the entire inner magnetosphere at a relatively high time cadence. For this study, a single example data-model comparison will be shown in order to highlight a few critical points.

The selected data for this comparison is a 10-minute integral image of hydrogen ENAs from 20:00 UT on April 17 in the 39–60 keV energy range. Plate 3 presents the data-model comparisons. Plates 3a and 3c show the equatorial plane hot ion fluxes from the Weimer-96 and self-consistent electric field simulations, respectively (averaged over pitch angle and energy in the 39–60 keV range). Plate 3b and 3d show the simulated ENA fluxes that HENA would have seen from the ion distributions in Plates 3a and 3c, respectively, by passing the ion fluxes through a forward-modeling routine (assuming pitch-angle isotropy and a dipole magnetic field). Plate 3e shows the HENA observations for this time and energy range. Note that the 3 ENA images in Plate 3 only show pixels in which the line of sight passes through the magnetic equatorial plane between 2 and 5.5 R_E geocentric distance. This truncation of the images focuses the presentation on the spatial region where the data-model comparison is most valid. For more details on the forward-modeling routine, please see *DeMajistre et al*. [2004]. For more details on the data-model comparison technique, please see *Liemohn et al*. [2005].

There are several features of Plate 3 that should be highlighted. One significant result is that the small scale features in the ion flux distribution of Plate 3c do not appear in the corresponding forward-modeled ENA flux distribution (Plate 3d). The lines of sight for each pixel pass through many flux tubes, and small-scale features are lost. The HENA image also shows no small-scale structure and it is likely that HENA cannot resolve it, so it cannot be used to prove or disprove the existence of these small-scale features.

A second point is that the ion flux values are very similar between the 2 simulations (compare Plates 3a and 3c). The self-consistent results have a flux peak in the evening sector and show significant structure while the Weimer results have a flux peak in the afternoon sector without much small-scale structure. The peak magnitudes, however, are almost identical.

A third point is that the simulated ENA fluxes from the self-consistent result (Plate 3d) are much closer in magnitude and morphology to the observed ENA fluxes (Plate 3e) than are those from the Weimer electric field simulation (Plate 3b). This isn't always the case (that is, for other times and energy channels, the results using the Weimer-96 field are sometimes a better match), but the example result shown in Plate 3 provides some amount of validation for the self-consistent result.

3. DISCUSSION

The purpose of this study was to assess the relative magnitude and the timing of the potential well-and-peak pairs

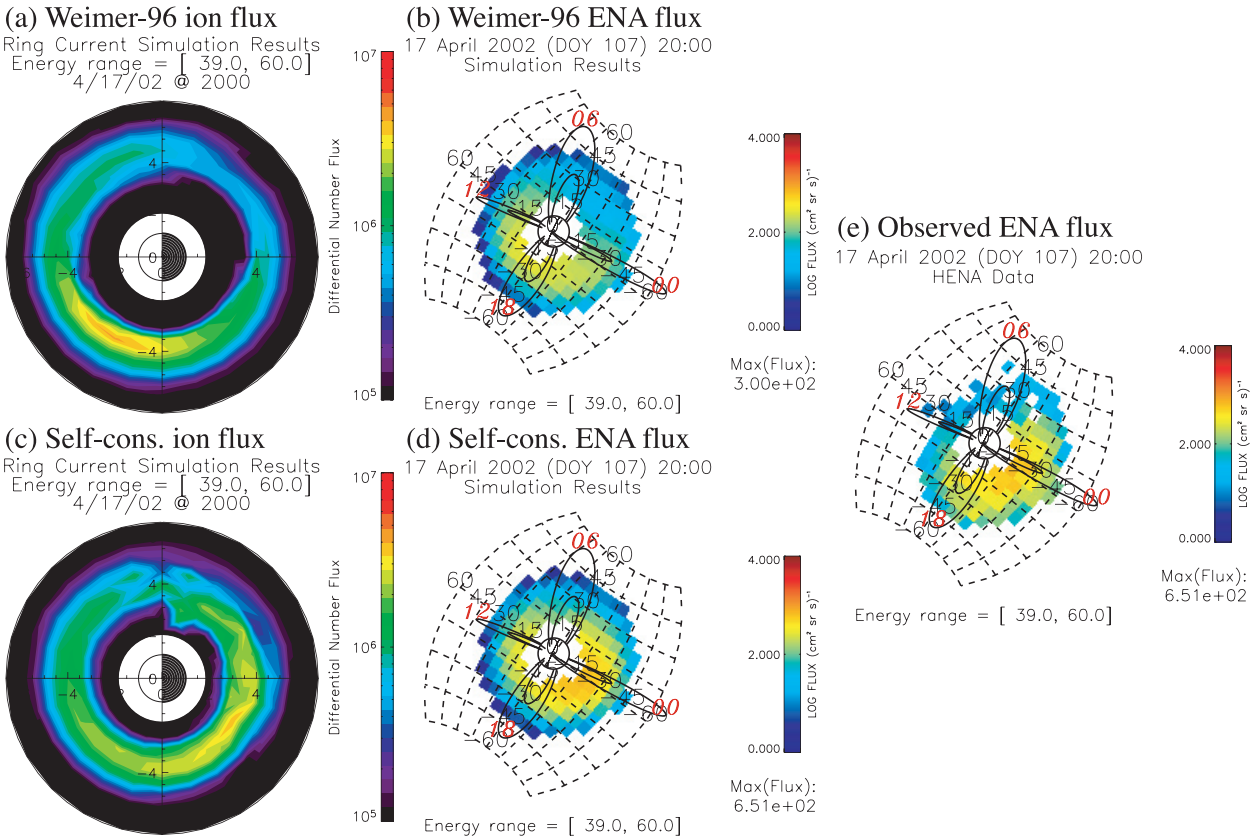

Plate 3. Data-model comparisons between RAM results and HENA observations for 20:00 UT on April 17. (a) Differential ion fluxes in the 39-60 keV energy range for the simulation with the Weimer-96 electric field description, and (b) the corresponding forward-modeled ENA fluxes from the IMAGE-HENA perspective. Similar plots for the simulation with the self-consistent electric field are shown in (c) and (d), respectively. Shown in (e) are the observed ENA fluxes from HENA for this energy channel. The ENA images only show pixels with lines of sight that cross the magnetic equatorial plane between 2 and 5.5 R_E geocentric distance. The is from over the North Pole and slightly anti-sunward, with the Sun direction to the left and slightly upward, as indicated.

generated around localized plasma pressure peaks in the inner magnetosphere. The answer is that they appear to always be important, as evidenced by the structure in the plasma pressure distributions plotted in Figure 1. However, they are not particularly visible in the potential pattern (at least on the chosen colorscale, with contours every 8 kV) when the large-scale convection field is strong. Furthermore, the resulting small-scale features in the ion flux and pressure distributions are not visible in the corresponding simulated ENA images.

The net effect of the self-consistent potential structures in the inner magnetosphere is that the injected plasma cannot simply convect around the duskside of the planet as a smooth and continuous pressure crescent. Some regions stagnate, others are pushed outward or inward, and still others are westwardly convected faster than expected. While the self-consistent electric fields are not strong enough to completely stop the large-scale Earthward flow of plasma sheet material into the inner magnetosphere, they are strong enough to destroy the coherence of the pressure peak. Potential vortices can exist right in the heart of the pressure peak and, assuming a certain conductance distribution in the inner magnetosphere, these potential well-and-peak pairs can significantly change the flow of plasma in the inner magnetosphere.

These differences in the hot ion pressure distribution between these two simulations are entirely consistent with the narrative in the previous section. The Weimer-96 potential model was compiled from observations but is sorted by solar wind and IMF conditions. Therefore, the transient, small-scale potential vortices associated with plasma injections are not resolved in the model. In fact, they largely cancel themselves out, because the injections can be localized or broad, and the plasma (and also the potential vortices) sweep through the inner magnetosphere.

Note that there can be very strong "inward" gradients in the potential in the self-consistent simulation (that is, westward flows). For instance, at 15:30, the electric fields in the evening sector near 4 R_E reach 3 mV/m, and they reach 2 mV/m at 16:30 and 18:30 UT. These strong dawn-dusk electric fields have been observed both in the topside ionosphere [*Yeh et al*., 1991; *Anderson et al*., 1991, 2001; *Foster and Vo*, 2002] and near the equatorial plane [*Rowland and Wygant*, 1998; *Wygant et al*., 1998; *Burke et al*., 1998]. They are so strong because at these places and at these times, a strong pressure-peak-induced flow is adding to a strong large-scale convection field. These regions of strong westward flow (that is, outward electric field in the magnetosphere) are known as sub-auroral polarization streams (SAPS) [*Foster and Burke*, 2002]. In these simulations, they are formed as a direct consequence of the additive superposition of the large-scale field and one of the small-scale fields in the inner magnetosphere during the storm. The SAPS can wax and wane and move around over the course of the storm, but the place where two fields add together to form the strongest westward drifts is near dusk.

Similarly, strong westward electric fields are occasionally generated in localized regions (particularly the evening sector) near the outer simulation boundary. This are exactly analogous to the "flow channels" described by *Chen et al*. [2003] and *Khazanov et al*. [2003, 2004] in both self-consistent electric field calculations and in AMIE potential distributions. Note that, in these simulation results, they are not induced electric fields formed by substorm dipolarizations, but rather potential electric fields formed by the additive effect of the large-scale field and a localized pressure peak field. In Figure 2, these flow channels are mainly seen in the evening sector and sometimes in the pre-dawn sector, just where they were seen in the previous studies.

It is interesting that the self-consistent potential pattern shows more fine-scale structure in the recovery phase than in the main phase (Figure 2). This is because some of the injected plasma is essentially trapped on the nightside, unable to convect sunward because of the pressure peak induced electric fields. There is a timescale for the nightside peak to eventually dissolve into a symmetric ring. In the meantime, though, the pressure peak is like a hydra: as the vortex flows break up one pressure peak, the result is two smaller peaks, each with their own vortex pairs. Westward drift is, of course, occurring throughout the storm (both main phase and recovery phase). The small-scale vortices simply alter these flows and hinder some of the plasma from completing its circuit.

Let us return to the schematic diagram of the process being discussed (Figure 1). The largest shaded region denotes the pressure peak (out to some arbitrary isobar). The partial ring current then flows westward in the outer half of this region and eastward in the inner half, turning around at each end. The inward-directed magnetic field gradient, however, means that the westward partial ring current is stronger than its eastward counterpart. The two smaller (and darker) shaded regions give the approximate locations of the FACs in to and out of the ionosphere that close the unbalanced portion of the partial ring current. There is a potential well coincident with the FACs flowing out of the ionosphere, and there is a potential peak coincident with the FACs flowing in to the ionosphere. Electric fields then radiate out from the potential peak and in towards the potential well. The resulting ExB drift is then a pair of vortex flows, counterclockwise around the well and clockwise around the peak. This is exactly like the high-latitude two-cell convection pattern formed by the region 1 current system, except these vortex pairs are much smaller. Right over the central region of the pressure peak is an outward flow where the two vor-

tices overlap. The strength of the vortices, of course depend on many factors, most notably the plasma intensity, energy and pitch angle distribution, and the ionospheric conductivity distribution. For the nominal conditions chosen for the simulation presented in this study, the vortices were strong enough to create significant and noticeable structure in the plasma pressure distribution in the inner magnetosphere throughout the storm event.

4. Conclusions

This study addressed the question of the timing and magnitude of the potential structures formed by the closure of the partial ring current. To investigate this issue, simulation results for the magnetic storm of April 17, 2002 were analyzed. It was found that the small-scale well-and-peak potential pairs, formed when magnetotail plasma is injected/convected in to the inner magnetosphere, significantly change the near-Earth pressure distribution. In particular, the main pressure peak is broken into many smaller peaks. The main phase asymmetric pressure peak also extends farther eastward towards dawn. In addition, relative to non-self-consistent results, the symmetric component of the ring current is larger in the main phase (although it is still smaller than the partial ring current) and the partial ring current is larger in the recovery phase (although it is still smaller than the symmetric ring current at this time). While the small-scale potential structures were not always visible in the plots, especially when the large-scale convection electric field was strong, the fine structure in the plasma pressure distribution was always visible. However, these features are not present in the simulated ENA images, and the HENA observations are also devoid of such features. Therefore, it is unresolved whether these small-scale structures in the hot ion distribution of the stormtime ring current are real. The magnitude and morphology of the simulated ENA fluxes are quite close to the observed values, though. This lends support to the concept of ring-current generated potential vortices inhibiting the rapid flow of particles through the inner magnetosphere.

The consequences of these partial ring current-induced potential structures were also discussed. In particular, SAPS and flow channels were seen in the potential distributions at various times during the storm. They form when the small-scale electric field is aligned with the large-scale electric field in some local region. The primary regions of formation (dusk and evening, respectively) are consistent with previous studies of these phenomena. While both the SAPS and flow channels wax and wane and move around throughout the event, they are a persistent feature of the stormtime potential pattern.

Acknowledgments. The authors would like to thank the sources of funding for this study: NASA grants NAG5-10297, NAG-10850, and NAG-12772 and NSF grants ATM-0090165 and ATM-0302529. Liemohn would also like to thank the organizers of the Yosemite 2004 Workshop for inviting him to present these results at the meeting. In addition, Liemohn thanks Drs. J. U. Kozyra, A. J. Ridley, and G. V. Khazanov for very useful discussions on this topic. Finally, we would like to thank all of the data providers who made the ring current simulations possible, especially M. F. Thomsen and G. D. Reeves at the Los Alamos National Laboratory, the Kyoto World Data Center for the Kp and Dst index, and CDAWeb for allowing access to the Level 2 plasma and magnetic field data of the ACE spacecraft (and to D. J. McComas and N. Ness for providing their data to CDAWeb).

REFERENCES

Akasofu, S.-I., and S. Chapman, On the asymmetric development of magnetic storm fields in low and middle latitudes, *Planet. Space Sci., 12*, 607, 1964.

Alfvén, H., and C.-G. Fälthammar, *Cosmical Electrodynamics*, Oxford University Press, London, 1963.

Anderson, P. C., W. B. Hanson, and R. A. Heelis, The ionospheric signatures of rapid subauroral ion drifts, *J. Geophys. Res., 96*, 5785, 1991.

Anderson, P. C., D. L. Carpenter, K. Tsuruda, T. Mukai, and F. J. Rich, Multisatellite observations of rapid subauroral ion drifts (SAID), *J. Geophys. Res., 106*, 29,599, 2001.

Banks, P. M., and G. Kokarts, *Aeronomy*, Parts A and B, Academic Press, New York, 1973.

Belian, R. D., G. R. Gisler, T. Cayton, and R. Christensen, High-Z energetic particles at geosynchronous orbit during the great solar proton event series of October 1989, *J. Geophys. Res., 97*, 16,897, 1992.

Brandt, P. C., S. Ohtani, D. G. Mitchell, M.-C. Fok, E. C. Roelof, and R. Demajistre, Global ENA observations of the storm mainphase ring current: Implications for skewed electric fields in the inner magnetosphere, *Geophys. Res. Lett., 29*(20), 1954, doi: 10.1029/2002GL015160, 2002.

Burch, J. L., IMAGE mission overview, *Space Sci. Rev., 91*, 1, 2000.

Burke, W. J., N. C. Maynard, M. P. Hagan, R. A. Wolf, G. R. Wilson, L. C. Gentile, M. S. Gussenhoven, C. Y. Huang, T. W. Garner, and F. J. Rich, Electrodynamics of the inner magnetosphere observed in the dusk sector by CRRES and DMSP during the magnetic storm of June 4-6, 1991, *J. Geophys. Res., 103*, 29,399, 1998.

Chen, M. W., M. Schulz, G. Lu, and L. R. Lyons, Quasi-steady drift paths in a model magnetosphere with AMIE electric field: Implications for ring current formation, *J. Geophys. Res., 108*(A5), 1180, doi: 10.1029/2002JA009584, 2003.

DeMajistre, R., E. C. Roelof, P. C:son Brandt, and D. G. Mitchell, Retrieval of global magnetospheric ion distributions from high-energy neutral atom measurements made by the IMAGE/HENA instrument, *J. Geophys. Res., 109*, A04214, doi: 10.1029/2003JA010322, 2004.

Ejiri, M., Trajectory traces of charged particles in the magnetosphere, *J. Geophys. Res., 83*, 4798, 1978.

Farley, D. T., A theory of electrostatic fields in a horizontally stratified ionosphere subject to a vertical magnetic field, *J. Geophys. Res., 64*, 1225, 1959.

Fejer, B. G., R. W. Spiro, R. A. Wolf, and J. C. Foster, Latitudinal variation of perturbation electric fields during magnetically disturbed periods: 1986 SUNDIAL observations and model results, *Ann. Geophys., 8*, 441, 1990.

Fok, M.-C., J. U. Kozyra, A. F. Nagy, C. E. Rasmussen, and G. V. Khazanov, Decay of equatorial ring current ions and associated aeronomical consequences, *J. Geophys. Res., 98*, 19,381, 1993.

Fok, M.-C., R. A. Wolf, R. W. Spiro, and T. E. Moore, Comprehensive computational model of Earth's ring current, *J. Geophys. Res., 106*, 8417, 2001.

Fok, M.-C., et al., Global ENA image simulations, *Space Sci. Rev.*, *109*, 77, 2003.

Foster, J. C., and H. B. Vo, Average characteristics and activity dependence of the subauroral polarization stream, *J. Geophys. Res., 107*(A12), 1475, doi: 10.1029/2002JA009409, 2002.

Foster, J. C., and W. J. Burke, SAPS: A new categorization for subauroral electric fields, *EOS Trans. AGU, 83*, 393, 2002.

Frank, L. A., Direct detection of asymmetric increases of extraterrestrial 'ring current' proton intensities in the outer radiation zone, *J. Geophys. Res., 75*, 1263, 1970.

Garner, T. W., R. A. Wolf, R. W. Spiro, W. J. Burke, B. G. Fejer, S. Sazykin, J. L. Roeder, and M. R. Hairston, Magnetospheric electric fields and plasma sheet injection to low L-shells during the 4–5 June 1991 magnetic storm: Comparison between the Rice Convection Model and observations, *J. Geophys. Res., 109*, A02214, doi:10.1029/2003JA010208, 2004.

Heppner, J. P., Polar cap electric field distributions related to the interplanetary magnetic field direction, *J. Geophys. Res., 77*, 4877, 1972.

Jaggi, R. K., and R. A. Wolf, Self-consistent calculation of the motion of a sheet of ions in the magnetosphere, *J. Geophys. Res., 78*, 2842, 1973.

Jordanova, V. K., L. M. Kistler, J. U. Kozyra, G. V. Khazanov, and A. F. Nagy, Collisional losses of ring current ions, *J. Geophys. Res., 101*, 111, 1996.

Jordanova, V. K., A. Boonsiriseth, R. M. Thorne, and Y. Dotan, Ring current asymmetry from global simulations using a high-resolution electric field model, *J. Geophys. Res., 108*(A12), 1443, doi: 10.1029/ 2003JA009993, 2003.

Khazanov, G. V., M. W. Liemohn, T. S. Newman, M.-C. Fok, and R. W. Spiro, Self-consistent magnetosphere-ionosphere coupling: Theoretical studies, *J. Geophys. Res., 108*(A3), 1122, doi: 10.1029/2002JA009624, 2003.

Khazanov, G. V., M. W. Liemohn, T. S. Newman, M.-C. Fok, and A. J. Ridley, Magnetospheric convection electric field dynamics and stormtime particle energization: Case study of the magnetic storm of 4 May 1998, *Ann. Geophys.*, *22*, 497, 2004.

Liemohn, M. W., J. U. Kozyra, V. K. Jordanova, G. V. Khazanov, M. F. Thomsen, and T. E. Cayton, Analysis of early phase ring current recovery mechanisms during geomagnetic storms, *Geophys. Res. Lett., 25*, 2845, 1999.

Liemohn, M. W., J. U. Kozyra, M. F. Thomsen, J. L. Roeder, G. Lu, J. E. Borovsky, and T. E. Cayton, Dominant role of the asymmetric ring current in producing the stormtime Dst*, *J. Geophys. Res., 106*, 10,883, 2001a.

Liemohn, M. W., J. U. Kozyra, C. R. Clauer, and A. J. Ridley, Computational analysis of the near-Earth magnetospheric current system, *J. Geophys. Res., 106*, 29,531, 2001b.

Liemohn, M. W., A. J. Ridley, D. L. Gallagher, D. M. Ober, and J. U. Kozyra, Dependence of plasmaspheric morphology on the electric field description during the recovery phase of the April 17, 2002 magnetic storm, *J. Geophys. Res., 109*(A3), A03209, doi: 10.1029/2003JA010304, 2004.

Liemohn, M. W., A. J. Ridley, P. C. Brandt, D. L. Gallagher, J. U. Kozyra, D. M. Ober, D. G. Mitchell, E. C. Roelof, and R. DeMajistre, Parametric analysis of nightside conductance effects on inner magnetospheric dynamics for the 17 April 2002 storm, *J. Geophys. Res.*, to be submitted, 2005.

McComas, D. J., S. J. Bame, B. L. Barraclough, J. R. Donart, R. C. Elphic, J. T. Gosling, M. B. Moldwin, K. R. Moore, and M. F. Thomsen, Magnetospheric plasma analyzer: initial three-spacecraft observations from geosynchronous orbit, *J. Geophys. Res., 98*, 13,453, 1993.

Mitchell, D. G., et al., High energy neutral atom (HENA) imager for the IMAGE mission, *Space Sci. Rev., 91*, 67, 2000.

Ober, D. M., J. L. Horwitz, and D. L. Gallagher, Formation of density troughs embedded in the outer plasmasphere by subauroral ion drift events, *J. Geophys. Res. 102*, 14,595, 1997.

Parker, E. N., Newtonian development of the dynamical properties of ionized gases of low density, *Phys. Rev., 107*, 924, 1957.

Parker, E. N., Newton, Maxwell, and magnetospheric physics, in *Magnetospheric Current Systems, Geophys. Monogr. Ser.*, vol. 118, ed. by S.-I. Ohtani, R. Fujii, M. Hesse, and R. L. Lysak, Am. Geophys. Un., Washington, D. C., p. 1, 2000.

Rairden, R. L., L. A. Frank, and J. D. Craven, Geocoronal imaging with Dynamics Explorer, *J. Geophys. Res., 91*, 13,613, 1986.

Ridley, A. J., T. I. Gombosi, and D. L. De Zeeuw, Ionospheric control of the magnetosphere: Conductance, *Ann. Geophys.*, *22*, 567, 2004.

Rowland, D., and J. R. Wygant, The dependence of the large scale electric field in the inner magnetosphere on magnetic activity, *J. Geophys. Res., 103*, 14,959, 1998.

Sazykin, S., R. A. Wolf, R. W. Spiro, T. I. Gombosi, D. L. De Zeeuw, and M. F. Thomsen, Interchange instability in the inner magnetosphere associated with geosynchronous particle flux decreases, *Geophys. Res. Lett., 29*(10), doi 10.1029/2001GL014416, 2002.

Southwood, D. J., and R. A. Wolf, An assessment of the role of precipitation in magnetospheric convection, *J. Geophys. Res., 83*, 5227, 1978.

Spiro, R. W., and R. A. Wolf, Electrodynamics of convection in the inner magnetosphere, in *Magnetospheric Currents*, Potemra, T. A., ed., p. 247. Amer. Geophysical Union, Washington, DC, 1984.

Spiro, R. W., R. A. Wolf, and B. G. Fejer, Penetration of high-latitude-electric-field effects to low latitudes during SUNDIAL 1984, *Ann. Geophys., 6*, 39, 1988.

Takahashi, S., T. Iyemori, and M. Takeda, A simulation of the storm-time ring current, *Planet. Space Sci., 38*, 1133, 1990.

Vasyliunas, V. M., Mathematical models of magnetospheric convection and its coupling to the ionosphere, in *Particles and Fields in the Magnetosphere*, edited by B. M. McCormac, p. 60, D. Riedel, Norwell, Mass., 1970.

Weimer, D. R., A flexible, IMF dependent model of high-latitude electric potentials having "space weather" applications, *Geophys. Res. Lett., 23*, 2549, 1996.

Wygant, J., D. Rowland, H. J. Singer, M. Temerin, F. Mozer, and M. K. Hudson, Experimental evidence on the role of the large spatial scale electric field in creating the ring current, *J. Geophys. Res., 103*, 29,527, 1998.

Yeh, H.-C., J. C. Foster, F. J. Rich, and W. Swider, Storm time electric field penetration observed at midlatitude, *J. Geophys. Res., 96*, 5707, 1991.

Young, D. T., H. Balsiger, and J. Geiss, Correlations of magnetospheric ion composition with geomagnetic and solar activity, *J. Geophys. Res., 87*, 9077, 1982.

P. C. Brandt, Johns Hopkins University, Applied Physics Laboratory, 11100 Johns Hopkins Road, Laurel, MD 20723 (pontus.brandt@jhuapl.edu).

M. W. Liemohn, Atmospheric, Oceanic, and Space Sciences Department, University of Michigan, 2455 Hayward St., Ann Arbor, MI 48109-2143 (liemohn@umich.edu).